Computational and Experimental Evidence for the Structural Preference of Phenolic C-8 Purine Adducts

Andrea L. Millen,[†] Christopher K. McLaughlin,[‡] Kewen M. Sun,[‡] Richard A. Manderville,*[,‡] and Stacey D. Wetmore*[,†]

Department of Chemistry, University of Lethbridge, 4401 University Drive, Lethbridge, Alberta, Canada, T1K 3M4, and the Department of Chemistry, University of Guelph, Guelph, Ontario, Canada, N1G 2W1

Received: December 24, 2007; In Final Form: February 2, 2008

The structural and spectral properties of (ortho and para) C8-aryl-purine adducts formed from carbon attachment by phenolic toxins were investigated through DFT calculations and UV−vis absorbance and emission studies. The global minima of both the deoxyadenosine (dA) and deoxyguanosine (dG) adducts adopted a syn conformation about the glycosidic bond due to the presence of an O5′−H···N3 hydrogen bond, where the anti minima are 20−30 kJ mol^{-1} higher in energy. While the nucleobase adducts are planar, the presence of the deoxyribose sugar induces a twist about the carbon−carbon bond connecting the phenol and nucleobase rings. ortho-Phenolic adducts are less twisted than the corresponding para adducts due to stabilization provided by an intramolecular O−H···N7 bond. Solvation calculations, in combination with UV−vis studies, demonstrate that the structural preference is solvent dependent, where solvents with hydrogen-bonding abilities disrupt the intramolecular O−H···N7 hydrogen bond such that a greater degree of twist is observed, and less polar solvents stabilize the planar structure. Indeed, the ratio of twisted to planar conformers is estimated to be as large as 50:50 in some aprotic solvents. Thus, the combined experimental and computational approach has provided a greater understanding of the structure of the ortho- and para-dA and dG C-bonded phenoxyl adducts as the first step to understanding the biological consequences of this form of DNA damage.

Introduction

DNA nucleobases can be modified to cultivate certain properties for use as bioprobes or designer molecules.[1−4] However, modified DNA also can arise as cellular damage due to, for example, oxidation,[5] deamination,[6] or alkylation[7] of the nucleobase. Other common damage products are bulky covalent adducts formed upon exposure to carcinogenic compounds found in the environment. Some chemicals can form covalent adducts directly, while others require metabolic activation.[8] Adduct structure can clarify the nature of the activated intermediates that have reacted with DNA to form the modified base. For example, C8-aryl-purine adducts[9−11] that arise from exposure to polycyclic aromatic hydrocarbons (PAHs),[12] aryl hydrazines,[10] and chloro-substituted phenols[13−15] stem from the intermediacy of radical species. Such radicals preferentially attach to the C8-site of purine nucleobases, as depicted in Scheme 1 for the reactivity of the phenolic radical with 2′-deoxyguanosine (dG).[16] For phenols[13−16] and PAHs,[12] peroxidase enzymes mediate radical formation, and therefore, C8-aryl-purine adducts may play a role in the carcinogenicity of phenols and PAHs in peroxidase-rich tissue.[12−16]

In the present study, we particularly were interested in phenolic adducts that stem from C-attachment and are structurally related to other C8-aryl-purine adducts formed from aryl hydrazines,[10,17,18] natural phenolic toxins,[9,15,16] and PAHs.[12] To understand the biological consequences that C8-aryl-purine adducts may induce, it is important to understand adduct structure. Indeed, the ortho-substituted dG adduct (**1**, Figure 1) has been synthesized previously, and its spectral properties studied, in attempts to gain information about the structure of this adduct.[19] It has been found that **1** can potentially exist in a planar enol conformation with an intramolecular hydrogen bond between the phenolic OH and the imine N (Scheme 2).[19] Phototautomerization of the planar structure through the ESIPT (excited-state intramolecular proton transfer) process to the keto form is recognizable by a large Stokes-shifted fluorescence.[19] Thus, ESIPT, coupled with the solvent dependence of this process, can be used to study the ground-state structural properties of the nucleoside. This structural analysis of **1** was based on similar studies of related compounds that are well-known to undergo ESIPT.[20−22]

SCHEME 1

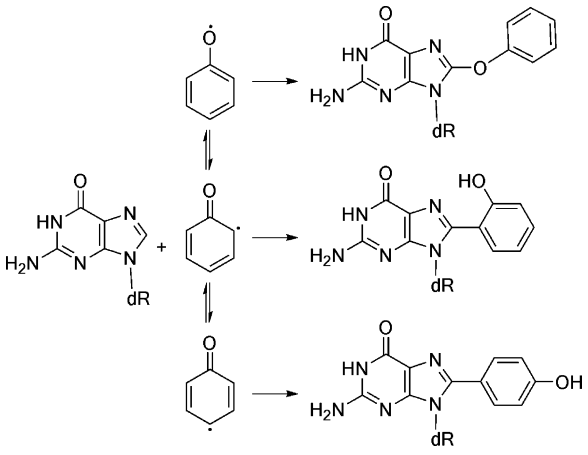

* To whom correspondence should be addressed. E-mail: (R.A.M.) rmanderv@uoguelph.ca and (S.D.W.) stacey.wetmore@uleth.ca.
[†] University of Lethbridge.
[‡] University of Guelph.

10.1021/jp712058a CCC: $40.75
Published on Web 04/01/2008

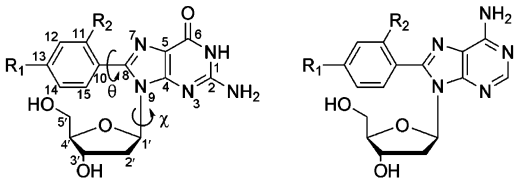

Figure 1. Structure, and atomic numbering, of ortho- and para-deoxyguanosine (**1** and **3**) and deoxyadenosine (**2** and **4**) C-bonded phenoxyl adducts and identification of dihedral angles χ ($\angle(O_4'C1'N_9C_4)$) and θ ($\angle(C_{11}C_{10}C_8N_9)$).

By analyzing the UV−vis absorbance and emission spectra for evidence of ESIPT, previous experimental studies concluded that **1** preferentially exists in a twisted conformation in most solvents, although a planar conformation also is present in some aprotic solvents.[19] However, similar studies on the nucleobase in the absence of the sugar moiety indicate that a planar structure is preferred, which suggests that the sugar may induce the twisted structure.[19] Indeed, previous studies have revealed that the sugar moiety affects the preferred nucleobase orientation in a unique class of modified nucleobases known as fleximers.[23]

The degree of flexibility and preferred conformation of **1** is explored further in the current work through detailed density functional calculations in the gas phase and in solution. Analogous computational studies, as well as new supporting experimental work, also will be presented for the 2′-deoxyadenosine (dA) ortho-C-adduct (**2**), as well as the dG (**3**) and dA (**4**) para-C-adducts. The corresponding deglycosylated analogues of **1**−**4** (denoted as deglyco**1**−deglyco**4**) also are considered to further evaluate the effects of the sugar moiety on the preferred nucleobase conformation in all adducts. Investigation of the dA ortho-C-adduct (**2**) will allow us to determine whether the composition of the nucleobase affects the preferred structure, while the para-phenolic C8 adducts of dG and dA are of interest due to their ability to act as fluorophores[24] and, therefore, their potential use as pH-sensing fluorescent probes.[24−27] Indeed, despite the potential importance of the para adducts, little is understood about their structure from previous work. The complementary experimental and computational approach taken in the present study reveals fundamental information about the structures of all adducts considered.

Computational and Experimental Methods

DFT Calculations. The B3LYP/6-311+G(2df,p)//B3LYP/6-31G(d) potential energy surfaces of deglyco**1**−deglyco**4** were considered as a function of θ, the dihedral angle that controls the relative orientation of the phenoxyl and nucleobase rings (Figure 1). In the ortho adducts (deglyco**1** and deglyco**2**), there exist two possible orientations of the phenol hydroxyl group, namely directed toward ($\angle(HOC_{11}C_{10}) = 0°$) and away from ($\angle(HOC_{11}C_{10}) = 180°$) the nucleobase. Since the relative energies indicate that the lowest energy structures involve the hydroxyl directed toward the nucleobase (Figures S1 and S2, Supporting Information), only this orientation will be further discussed for all ortho adducts.

Because of the inherent flexibility within **1**−**4**, the corresponding potential energy surfaces are complicated. Specifically, the sugar puckering and the orientation of the nucleobase about the glycosidic bond (defined by the dihedral angle χ, Figure 1) must be considered in addition to rotation about θ. Therefore, systematic B3LYP/6-31G(d) potential energy surface scans were

SCHEME 2

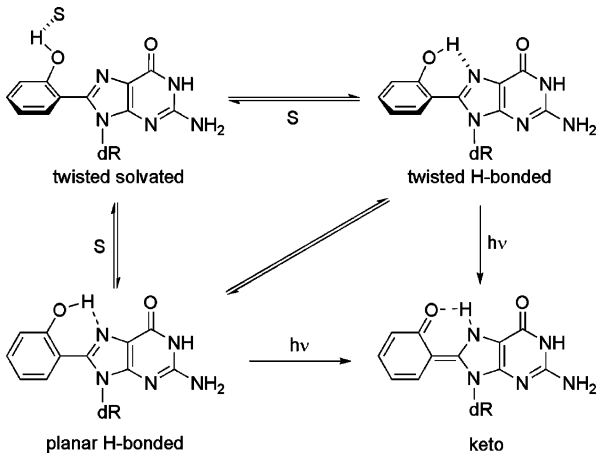

performed where the dihedral angles referred to as χ and θ (Figure 1) were constrained in 10° increments from 0 to 360°. Because of the large number of conformations associated with the sugar moiety and our primary interest in the effects of the sugar moiety on the structure of the nucleobase, preliminary conformational searches were performed using Monte Carlo with MMFF as implemented in the Spartan[28] software package to identify the preferred sugar conformation.[29] The 10 lowest energy structures identified from these scans were subsequently optimized with B3LYP/6-31G(d). For both the para and the ortho adducts, the lowest energy conformer involves C2′−*endo* sugar puckering, which is the puckering present in B-DNA. Additionally, the C5′ hydroxyl group is directed toward the nucleobase, where further test calculations on B3LYP optimized geometries support that this dihedral angle is generally preferred over others due to interactions between C5′ hydroxyl hydrogen and O4′ or the nucleobase. Finally, the C3′ hydroxyl group is directed toward C2′ ($\angle$(HC3′OH) is approximately −60°) for all structures. We note that one conformer of the ortho-adenine adduct identified from Spartan conformational searches has a different orientation of the C3′ hydroxyl group; however, this structure is only 0.5 kJ mol^{-1} lower in energy than that with the −60° orientation, and the three other adducts all prefer the −60° orientation.

On the basis of the results from the conformational searches, three additional selection rules for the geometries of **1**−**4** were used during the B3LYP/6-31G(d) scans. First, the sugar puckering was constrained to C2′−*endo*, where preliminary studies on the corresponding (ortho) damaged imidazole nucleoside revealed that the correct minima were obtained by initially constraining the sugar puckering and subsequently releasing the constraint to yield more accurate energies. Second, although the orientations of the hydroxyl groups were not constrained, only structures with a $\angle$(HC3′OH) dihedral angle of approximately −60° and the C5′ hydroxyl group directed toward the nucleobase (i.e., a $\angle$(C4′C5′OH) dihedral angle of approximately 50−90°) were considered.

To more accurately determine the geometries and relative energies of the minima and transition states identified from the potential energy surface scans for **1**−**4**, full optimizations (i.e., all constraints released) were subsequently performed. Higher level (B3LYP/6-311+G(2df,p)) single-point calculations were performed in the gas phase on all fully optimized structures. Additionally, PCM single-point calculations, as well as full optimizations, were performed on the lowest energy structures in various solvents (cyclohexane, chloroform, acetonitrile, DMSO, and water), which represent the range in polarities and

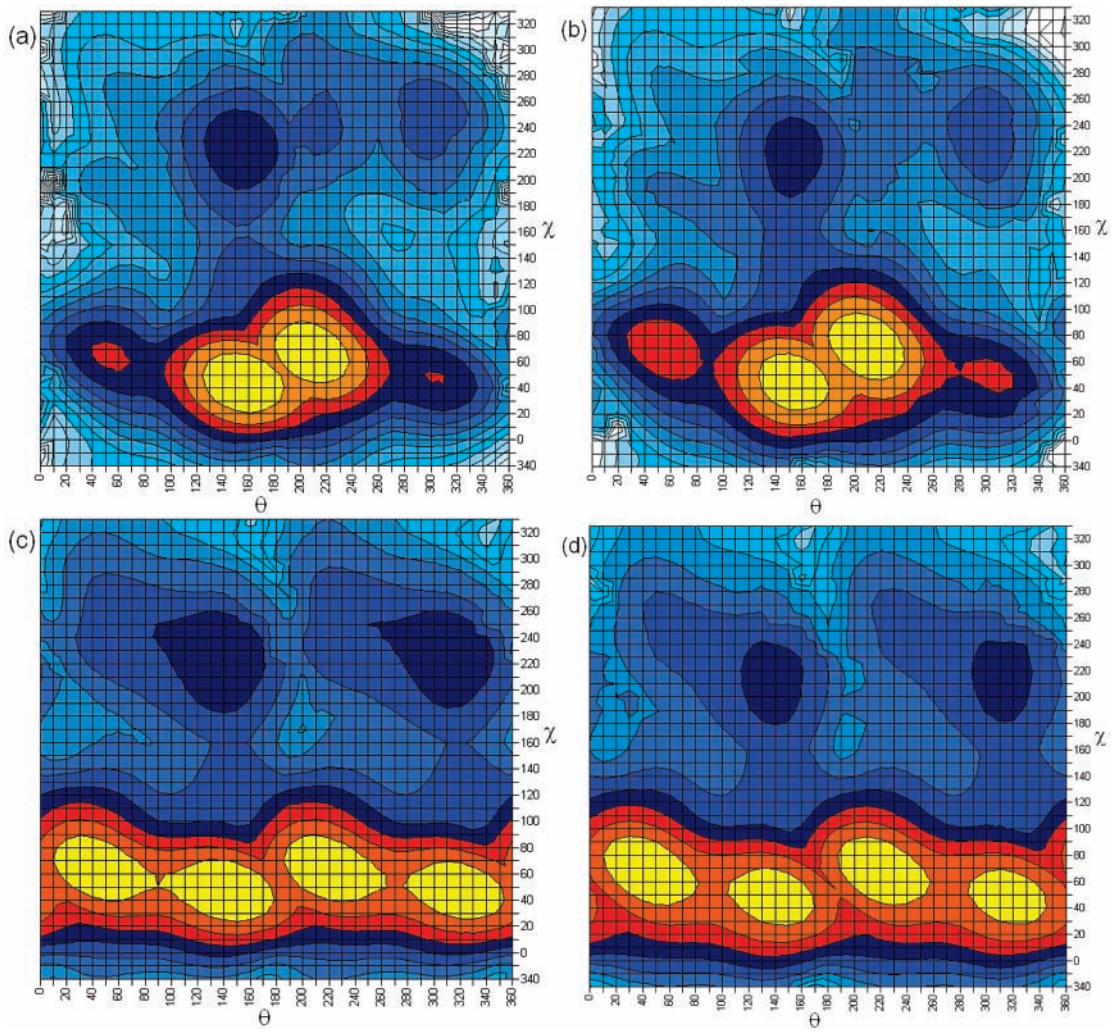

Figure 2. B3LYP/6-31G(d) potential energy surface for (a) ortho-deoxyguanosine (**1**), (b) ortho-deoxyadenosine (**2**), (c) para-deoxyguanosine (**3**), and (d) para-deoxyadenosine (**4**) C-bonded phenoxyl adducts with θ plotted along the *x*-axis, χ plotted along the *y*-axis, and energy represented by color, where yellow represents the lowest energy regions, and each change in color represents an increase in the relative energy of 10 kJ mol^{-1}.

solvents used in our experiments. All B3LYP calculations were performed using Gaussian 03.[30]

General Experimental Methods. ^{1}H NMR spectra were recorded on a Bruker Avance 300 DPX or Bruker Avance 400 DPX operating at 300.1 and 400.1 MHz, respectively, and ^{13}C NMR spectra were recorded on a Bruker Avance 300 DPX operating at 75.5 MHz. ^{1}H NMR spectra were referenced to the residual proton solvent signal of the deuterated solvent, and ^{13}C NMR spectra were referenced to the ^{13}C NMR resonance of the deuterated solvent. All ^{13}C NMR spectra were acquired using the J-modulated (JMOD) pulse sequence.[31]

Unless otherwise noted, commercial compounds were used as received. Boronic acids were purchased from Sigma-Aldrich. $Pd(OAc)_2$ was purchased from Strem Chemical, and dG was from ChemGenes. Formic acid was obtained from Sigma-Aldrich. The syntheses of 8-BrdG[32] and 8-BrdA[33] were performed according to literature methods. High-resolution mass spectrometry (HRMS) was conducted at the McMaster Regional Centre for Mass Spectrometry, Hamilton, ON, and spectra were obtained on a Micromass/Waters Global Ultima quadrupole time-of-flight mass spectrometer using electrospray negative ionization at a resolving power of ~8000 W.

UV−vis spectra were recorded on a Cary 300-Bio UV−vis spectrophotometer equipped with a Peltier block-heating unit, stirrer, and temperature controller. Fluorescence emission and excitation spectra were obtained on a Cary Eclipse fluorescence spectrophotometer. Standard 10 mm light path quartz glass cells from Hellma GmbH and Co. were used. Unless otherwise specified, all UV−vis spectra were recorded at 25 °C with baseline/background correction and stirring. Fluorescence measurements were observed after excitation at the compounds' absorbance maxima with emission observed from 10 nm above the excitation wavelength (to a minimum of 300 nm) to 600 nm. Quinine bisulfate·H_2SO_4 was obtained from Alfa Aesar and used without purification. Solvents used were of spectroscopic grade. Because of their sparing solubility in other solvents, all stock solutions of adducts **1**−**4** and deglyco**1**−deglyco**4** were prepared in DMSO, requiring that experimental spectroscopic solutions contain ≤1% DMSO by volume. Any water used for buffers or spectroscopic solutions was obtained from a MilliQ filtration system (18.2 MΩ). All solutions were syringe-filtered with 0.2 μm PTFE filters from Mandel Scientific. pH measurements were taken at room temperature with an Accumet AP63 Handheld pH meter via a 1.5 in. Accumet Combination Micro Electrode with stirring. Quantum yield values for adducts **1**−**4** and deglyco**1**−deglyco**4** were determined in MOPS buffer (10 mM, pH 7, 0.1 M NaCl) using the comparative method with quinine bisulfate ($\Phi_{fluor} = 0.546$ with excitation at 294 nm) in 0.5 M H_2SO_4 acting as a fluorescence quantum yield standard.[19,34]

General Method for Metal-Mediated Arylation of 8-BrdG and 8-BrdA. These reactions were conducted according to the literature and are briefly described here.[19,24,35] Palladium acetate (2.2 mg, 0.01 mmol), tris-(*m*-sulfonatophenyl)phosphine trisodium (TPPTS) (14.8 mg, 0.025 mmol), sodium carbonate (80 mg, 0.75 mmol), 8-BrdG (0.375 mmol), and the appropriate boronic acid (0.45 mmol) were added to degassed 2:1 water/acetonitrile (3.5 mL) and heated to 80 °C for 4 h under an argon balloon. The reaction was diluted with ca. 20 mL of water, and the pH was adjusted to 6−7 with 10% HCl (aq). The mixture was allowed to cool to 0 °C for several hours before the product was recovered by vacuum filtration. Using this procedure, adducts **1**,[19] **3**,[24] and **4**[24] were previously reported by us.

8-(2″-Hydroxyphenyl)-2′-deoxyadenosine (2). Adduct **2** was synthesized from 8-BrdA (0.665 g, 2.01 mmol), 2-hydroxyphenyl boronic acid (301 mg, 2.18 mmol), $Pd(OAc)_2$ (12.6 mg, 0.019 mmol), TPPTS (65 mg, 0.114 mmol), and Na_2CO_3 (395 mg, 3.73 mmol) as outlined in the general procedure. This adduct was extracted with EtOAc (3 × 100 mL) after an adjustment of the pH to 6−7. Any precipitate that had formed after the reaction mixture had cooled to room temperature was filtered from the reaction mixture before EtOAc extraction. The combined organic extracts were dried over Na_2SO_4, and the organics were removed under reduced pressure to yield **2** as a white powder (0.50 g, 73%). UV−vis (MOPS) λ_{max} 270 nm, ϵ_{270} 17 037 cm^{-1} M^{-1}; ^{1}H NMR (DMSO-d_6) (300 MHz), δ: 10.25 (s, 1H, C2″OH), 8.11 (s, 1H, H), 7.40 (brs, 2H, NH_2), 7.37 (bm, 2H, H3″, H5″, overlapped with previous peak), 5.93 (dd, 1H, J = 6.0, 8.7 Hz, H1′), 5.84 (m, 1H, 5′OH, overlapped with previous peak), 5.21 (d, 1H, J = 3.9 Hz, 3′OH), 4.40 (m, 1H, H3′), 3.81 (brs, 1H, H4′), 3.36, 3.53 (bm, 2H, H5″, H5′), 3.10 (m, 1H, H2″), 2.16 (m, 1H, H2′); HRMS calcd for $C_{16}H_{17}N_5O_4$ $[M + H]^+$ 344.1349, found 344.1355.

Deglycosylation. Deglycosylation of adducts **1**−**4** to afford guanine and adenine analogues deglyco**1** to deglyco**4** was achieved by placing nucleosides in ca. 20 mL of 10% formic acid under heat (75 °C) for 1 h, as outlined previously for deglyco**1**.[19] After cooling, the reaction mixtures were brought to pH 6 with 1 N NaOH, and adduct nucleobases were recovered by crystallization and filtering from the aqueous media. ^{1}H NMR analyses showed that this procedure of deglycosylation generated a single adenine nucleobase and two guanine nucleobases that were ascribed to two enol tautomers.[19] As reported previously for deglyco**1**,[19] NMR analyses of deglyco**3** did not permit unambiguous assignment of the guanine adduct structures. Peak assignments for the major tautomer of deglyco**3** (∼70%) are given. ^{1}H NMR spectra of adduct **2** (Figure S3) and deglyco**2** to deglyco**4** (Figures S4−S6) are available in the Supporting Information.

8-(2″-Hydroxyphenyl)-adenine (Deglyco2). Deglyco**2** was recovered as a byproduct of the synthesis of **2**, and as such, no treatment with acid and heat was required. UV−vis (MOPS) λ_{max} 317 nm, ϵ_{317} 14 369 cm^{-1} M^{-1}; ^{1}H NMR (DMSO-d_6) (300 MHz), δ: 13.6 (br s, 1H, N9H), 12.62 (br s, 1H, C2″-OH), 8.17 (s, 1H, H), 8.01 (d, 1H, J = 7.5 Hz, 1H), 7.43 (br s, 2H, NH_2), 7.35 (m, 1H, overlapped with previous peak), 6.98 (m, 2H).

8-(4″-Hydroxyphenyl)-guanine (Deglyco3). Starting from **3** (0.200 g, 0.56 mmol), deglyco**3** was obtained as a white solid (0.109 g, 80%); UV−vis (MOPS) λ_{max} 309 nm, ϵ_{309} 19 953 cm^{-1} M^{-1}; ^{1}H NMR (DMSO-d_6) Major species (70%) δ 12.5 (s, 1H), 10.47 (s, 1H), 9.76 (s, 1H), 7.79 (d, J = 8.8 Hz, 2H), 6.81 (d, 2H, major/minor peaks together), 6.31 (s, 2H).

8-(4″-Hydroxyphenyl)-adenine (Deglyco4). Starting from **4** (0.100 g, 0.29 mmol), deglyco**4** was obtained as a white solid (0.053 g, 80%); UV−vis (MOPS) λ_{max} 302 nm, ϵ_{302} 18 197 cm^{-1} M^{-1}; ^{1}H NMR (DMSO-d_6) δ 13.51 (br s, 1H), 9.90 (s, 1H), 8.05 (s, 1H), 7.93 (d, J = 8.5 Hz, 2H), 7.01 (s, 2H), 6.85 (d, J = 8.5 Hz, 2H).

Results

ortho-C-Bonded Adducts. *(i) Nucleoside.* We begin our discussion by considering the electronic structure of the ortho-C-bonded phenoxyl adducts of deoxyguanosine (**1**) and deoxyadenosine (**2**). Figures 2a,b display the results from the B3LYP potential energy surface scans for **1** and **2**, where θ and χ were held fixed in 10° increments from 0 to 360°. Although we feel confident that we have properly characterized the minima on these surfaces, close atomic contacts make it difficult to find stable structures in the white regions of the graphs. We anticipate that the corresponding high-energy structures do not play a significant role, and therefore, we focus our attention on the more stable regions of the surface.[36]

The orientation of the nucleobase about the glycosidic bond can be categorized as anti or syn according to χ, where anti is defined by χ values ranging from 90 to 270°, and syn refers to χ values of 0−90 and 270−360°. The contour plots for **1** and **2** reveal that the global minima (yellow region) adopt a syn orientation. Indeed, there are four syn minima (χ ranging from 40 to 70°) that are all lower in energy than any anti minima. This is particularly interesting since natural nucleobases adopt the anti orientation, which is required to form Watson−Crick hydrogen bonds with the neighboring DNA strand. Nevertheless, our findings are in agreement with previous computational and experimental studies for other unnatural bases,[37] including other C8-bonded purine adducts.[38−40] The anti region of the graphs displays less smooth surfaces in part due to steric crowding as the phenol ring passes over the sugar moiety. However, two anti minima can be identified, which are at least 30 kJ mol^{-1} higher in energy than the syn global minimum. Rotational barriers between minima also can be estimated from the graph to be approximately 30−40 (20−30) kJ mol^{-1} for conversion between syn (anti) minima and 50−80 kJ mol^{-1} for syn to anti conversions.

When full optimizations (i.e., all constraints released) are performed on points of interest from the contour plots, the geometries change very little, where χ and θ deviate by less than 5° in minima (16° in transition states). The sugar puckering also generally remains C2′−*endo*; however, more significant deviations occur in some instances, which will be discussed in more detail below. Important geometrical parameters, as well as the relative energies, for fully optimized minima and transition states are provided in Figures 3 and 4.

All syn minima contain a strong O5′−H···N3 hydrogen bond (1.80−1.96 Å), and the phenoxyl substituent is twisted with respect to the nucleobase, where the magnitude of the twist depends on favorable intramolecular interactions and steric considerations. For example, in the global minimum ($\chi \approx 70°$ and $\theta \approx 205°$), and a nearly thermoneutral local minimum ($\chi \approx 45°$ and $\theta \approx 155°$), the phenoxyl substituent is twisted out of the plane of the nucleobase by approximately 20−30°. Despite this twisting, both structures contain an O−H···N7 hydrogen bond (1.77−1.82 Å), where the phenol hydrogen moves 10−13° out of the plane of the ring to maintain this (albeit slightly twisted) interaction. In the global minimum, the phenol ring is twisted such that a phenol hydrogen is closer to O4′ and steric crowding between hydrogen atoms in the sugar

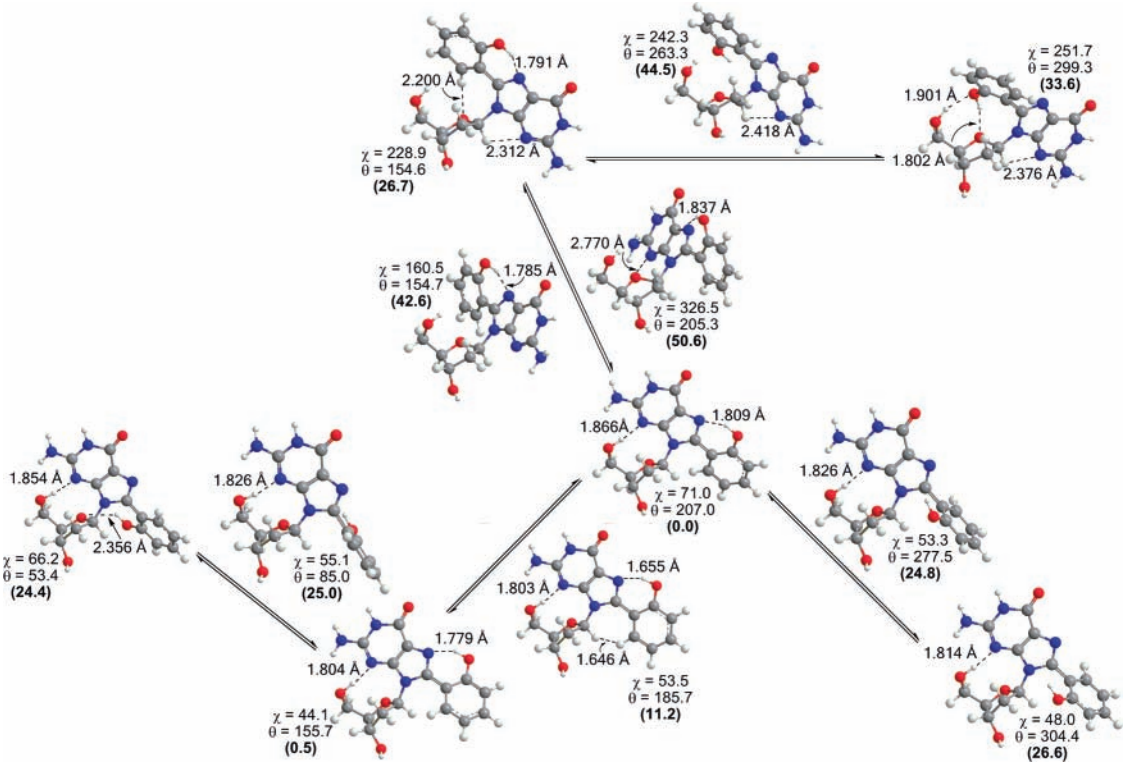

Figure 3. Selected bond lengths (Å) and dihedral angles (χ and θ, deg) for the minima and transition states of the C-bonded ortho-deoxyguanosine phenoxyl adduct (**1**) fully optimized with B3LYP/6-31G(d) (relative energies from B3LYP/6-311+G(2df,p) single-point calculations provided in parentheses, kJ mol^{-1}).

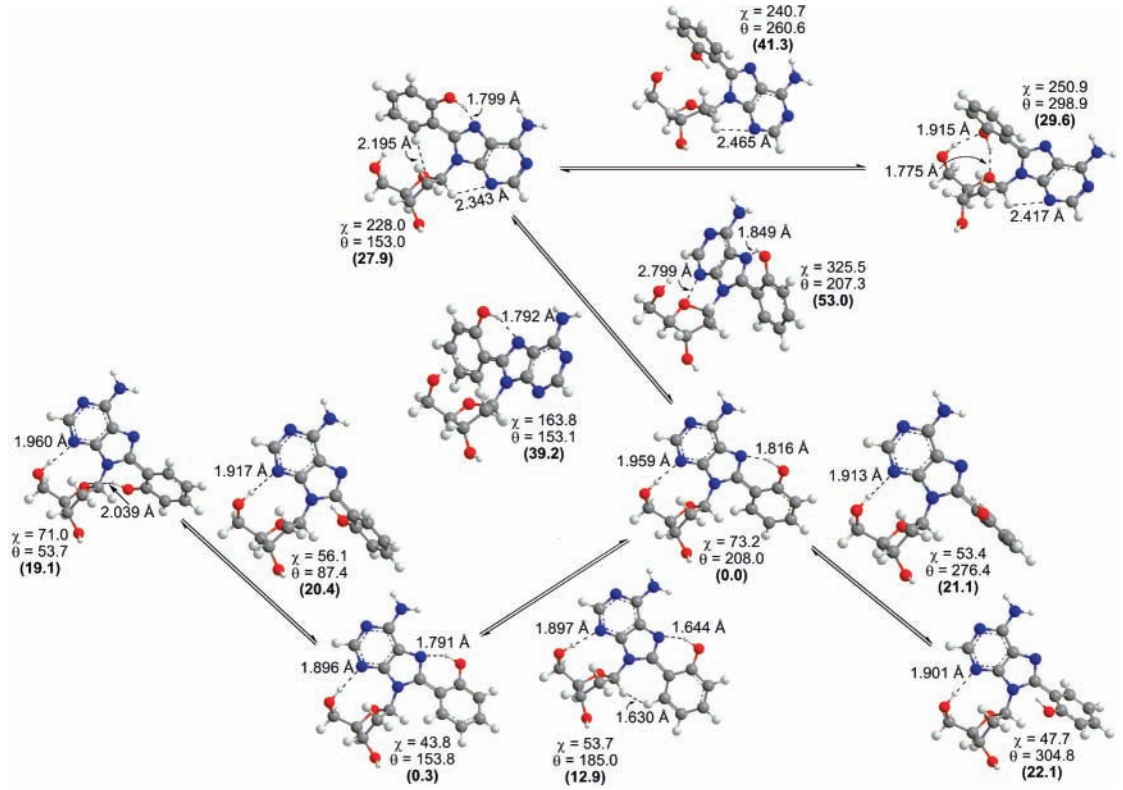

Figure 4. Selected bond lengths (Å) and dihedral angles (χ and θ, deg) for the minima and transition states of the C-bonded ortho-deoxyadenosine phenoxyl adduct (**2**) fully optimized with B3LYP/6-31G(d) (relative energies from B3LYP/6-311+G(2df,p) single-point calculations provided in parentheses, kJ mol^{-1}).

(C1′ and C2′) and the phenol is reduced. In two secondary (syn) local minima ($\chi \approx 70°$ and $\theta \approx 55°$ and $\chi \approx 50°$ and $\theta \approx 305°$), the phenoxyl ring is twisted by as much as 50° to avoid repulsive interactions between the phenol hydroxyl hydrogen and the C1′ of the sugar. The structure with $\theta \approx 55°$ is 3 kJ mol^{-1} more stable than that with $\theta \approx 305°$ due to a weak O−H···O4′ hydrogen bond and reduced steric crowding between the C2′ and the phenol hydrogens.

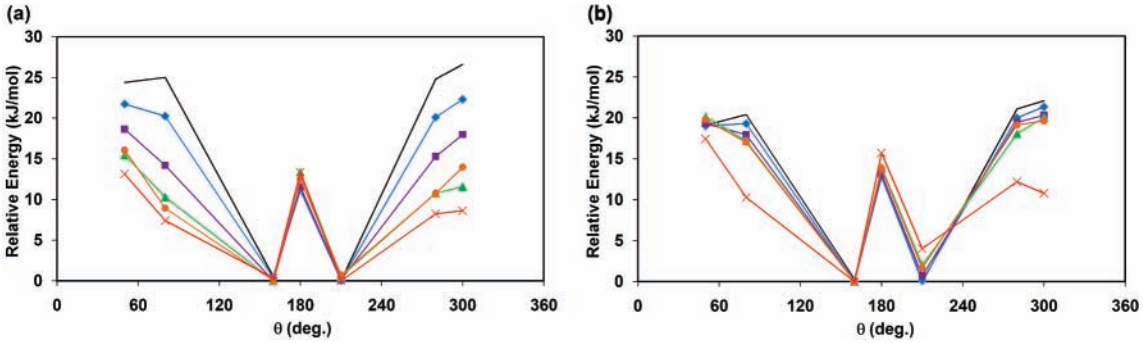

Figure 5. B3LYP/6-311+G(2df,p) relative energies of syn minima and transition states in gas phase (black, no symbol), cyclohexane (blue, ◆), chloroform (purple, ■), acetonitrile (green, ▲), DMSO (orange, ●), and water (red, ×) for (a) **1** and (b) **2** (see Figures 3 and 4 for geometrical information).

The conformation of **1** and **2** with a planar nucleobase and strong O−H···N7 hydrogen bond ($\theta \approx 180°$) was found to be a transition state that connects two twisted minima. This is due to repulsive interactions between a phenoxyl C_{15}−H hydrogen and C1′−H, which were reduced by twisting about θ. Nevertheless, the energy barrier for rotation about θ is small (11−13 kJ mol^{-1}), which suggests that rotation between the two twisted minima will readily occur and that environmental effects could be sufficient to stabilize the planar structure. The remaining two syn transition states contain a perpendicular arrangement of the nucleobase and phenol rings.

Two anti local energy minima ($\chi \approx 230-250°$) contain interactions between the C5′ hydroxyl and the π-system ($\theta \approx 160°$) or the hydroxyl group ($\theta \approx 300°$) of the phenoxyl substituent. These interactions lead to steric crowding, which is partially alleviated due to changes in the sugar puckering to the C1′−*exo*−C2′−*endo* twist. As found for the (syn) global minimum, the lowest energy anti minimum contains an O−H···N7 hydrogen bond, and the phenol ring is twisted by approximately 20° about θ. Nevertheless, this anti structure is 20−30 kJ mol^{-1} higher in energy than the syn structures due to the absence of the strong O5′−H···N3 hydrogen bond. The anti minima are connected by a transition state at $\chi \approx 240°$ and $\theta \approx 260°$, which has C1′−*exo*−C2′−*endo* twist sugar puckering and is approximately 40−45 kJ mol^{-1} above the syn global minima.

Two transition states between anti and syn regions of the surface also were characterized ($\chi \approx 160°$ and $\theta \approx 155°$ and $\chi \approx 325°$ and $\theta \approx 205°$), which both contain O−H···N7 hydrogen bonds, and the phenoxyl hydrogen is located approximately 15° out of the phenyl plane. Although the transition state at $\chi \approx 160°$ has predominately C2′−*endo* sugar puckering, the structure at $\chi \approx 325°$ has a C1′−*exo*−C2′−*endo* twist conformation and is distorted about the glycosidic bond due to repulsion between N3 and O4′. The corresponding barriers (40−53 kJ mol^{-1}) indicate that although rotation about χ is more difficult than rotation about θ, the anti region of the conformational space will be sampled.

Our calculations suggest that the potential energy surfaces for **1** and **2** are very similar. Although both have four minima in the syn region, the syn surface for **2** is shallower due to weaker (longer) O−H···N7 and O5′−H···N3 hydrogen bonds in **2** as compared to **1**. Similarly, differences in the anti regions of the graphs can be attributed to weaker C1′−H···N3 hydrogen bonds in **2**. Despite these subtle differences, the geometries for the minima and transition states for the dA and dG adducts are nearly identical.

The most important conclusion from the structures discussed thus far is that the lowest energy conformations involve a twisted arrangement of the phenoxyl substituent relative to the nucleobase ring in the gas phase. However, previous experimental studies on **1** considered a wide range of solvents and determined a solvent dependence for the preferred structure.[19] Therefore, it is of interest to determine the environmental effects on our results. Since solvation is not expected to provide sufficient stabilization to introduce a preference for the anti structures, B3LYP/6-311+G(2df,p) PCM single-point calculations were performed in various solvents (hexane, chloroform, acetonitrile, DMSO, and water) on the four minima and three transition states in the syn region of the potential energy surface (Figure 5).

Although the energy differences are small, solvation single-point calculations on gas-phase geometries indicate that the potential energy surfaces change in different environments. Specifically, the planar transition structure ($\theta = 180°$) is destabilized, and the twisted structures are stabilized, as the polarity of the solvent increases. This trend can be most clearly seen for the dG adduct (**1**), but also holds for the corresponding dA adduct (**2**). Free optimizations in solution show that the geometries actually change very little, and the same trends in the relative energies are seen upon full optimization as reported for the single-point calculations (see Table S1, Supporting Information, for relative energies and geometrical information obtained upon full optimization in various solvents). There is, however, a slight tendency toward more planar structures upon optimization in solvents with a low polarity, as suggested by the single-point calculations. We note that only single-point data are presented in the text since some solvation optimizations failed to converge, and single-point calculations on gas-phase geometries yielded the same trends when optimized geometries were obtained in solution.

Our calculations are supported by UV−vis spectra obtained for **1** and **2** in a range of aprotic solvents (Figure 6), as well as the corresponding optical data in water (Table 1). Specifically, a previous study assigned absorbance at ∼280 nm in the spectra of **1** to a twisted enol tautomer and absorbance at ∼320 nm to a planar conformation of the nucleobase containing an O−H···N7 hydrogen bond.[19] These assignments were made based on the fact that a planar conformation with an O−H···N7 hydrogen bond can phototautomerize through ESIPT to the keto form (Scheme 2). As highlighted in Figure 7 for the absorbance and emission spectra of adducts **1** and **2** in buffered water and hexane, the keto structure is identifiable by a large Stokes-shifted fluorescence (emission at ∼470 nm in hexane as compared to emission at ∼390 nm for the enol tautomer in water, Figure 7). Given the structural similarities between **1** and **2** as identified from our computational studies, these peak assignments also can be applied to the dA adduct in the present study (Figure 7b). However, we note that in water at pH 7, the

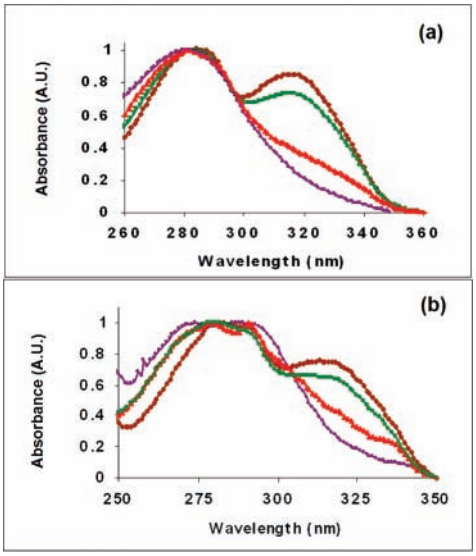

Figure 6. Overlay of UV−vis absorbance spectra for adducts (a) **1** and (b) **2** in $CHCl_3$ (◆, brown), MeCN (■, green), hexane (▲, bright red), and DMSO (●, purple).

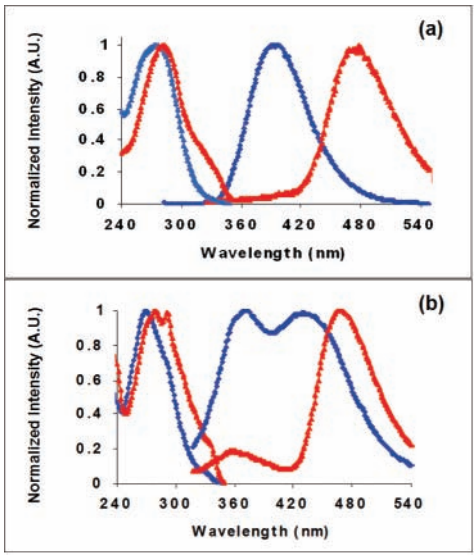

Figure 7. Normalized absorbance and emission spectra for adducts (a) **1** and (b) **2** in buffered water (MOPS), 10 mM, pH 7, 0.1 M NaCl (◆, blue) and hexane (▲, bright red).

emission of **2** shows two maxima: a blue-shifted peak (∼374 nm) that is ascribed to the enol structure and a second emission at ∼447 nm (Figure 7b and Table 1). We conclude that the red-shifted emission for **2** is due to the phenolate since increasing the pH to 11 generates preferential emission at 447 nm. Formation of the phenolate also is consistent with the observed drop in quantum yield for **2** (Table 1) since we have previously demonstrated that the fluorescence intensity of the para-dA adduct **4** is quenched upon the addition of base and the formation of the phenolate.[24]

Figure 6 shows that in acetonitrile and chloroform, the absorbance spectra of **1** and **2** contain two peaks at ∼280 and 320 nm, which indicates that both twisted and planar structures are present. The relative peak heights suggest that the planar conformation is present in higher concentrations in chloroform than acetonitrile and that the planar conformation is present in even lower concentrations in hexane. In solvents with high polarities (DMSO), the absorbance spectra of **1** and **2** contain only one peak at ∼280 nm, which indicates the presence of a twisted enol structure that cannot phototautomerize. Indeed,

TABLE 1: Photophysical Data for Adducts 1−4 and Deglyco1−4

adduct	λ_{max} (nm), log ϵ[a]	λ_{em} (nm)	Φ_{fl} [a]
1[b]	276, 4.25	395	0.44
2	270, 4.23	374, 447	0.04
3[c]	278, 4.26	390	0.47
4[c]	282, 4.27	391	0.56
deglyco**1**[b]	319, 4.28	393	0.20
deglyco**2**	317, 4.16	446	0.05
deglyco**3**	309, 4.30	388	0.45
deglyco**4**	302, 4.26	372	0.44

[a] 10 mM MOPS buffer, pH 7.0, μ = 0.1 M NaCl. [b] See ref 19. [c] See ref 24.

studies on **1** and **2** in water (Table 1) also show only one absorbance peak at ∼280 nm, where it was previously proposed that the O−H···N7 hydrogen bond in **1** is broken in hydrogen-bonding solvents such that only a twisted (non-hydrogen bonded) enol structure is present.[19]

Thus, the calculated trend with respect to solvation is in agreement with experiments. Specifically, both single-point calculations (Figure 5) and full optimizations (Table S1, Supporting Information) indicate that the twisted conformer is stabilized in solvents with a high polarity (DMSO, water), while the stability of the planar structure increases with a decrease in the dielectric (polarity) of the solvent. We propose that whether the twisted and/or planar nucleobase conformations are observed is due to a balance between the steric effects of the sugar, which influences the twist of the nucleobase, and the strong O−H···N7 hydrogen bond, which anchors the nucleobase in a planar conformation. Our experimental and computational results imply that as the polarity of the solvent increases, the strength of the hydrogen bond weakens, and therefore, the steric interactions become predominant or, in other words, the twisted structure becomes more favorable. This will especially be true in solvents that are capable of forming discrete hydrogen bonds and thereby break the O−H···N7 interaction altogether. This argument also explains the difference in the calculated solvent effects on the relative energies of **2** as compared with **1** (Figure 5). Specifically, since the O−H···N7 hydrogen bond of **2** is weaker than **1 (**Figures 3 and 4), the effect of the solvent polarity on the strength of the hydrogen bond is less significant in **2**.

(ii) Nucleobase. To further understand the steric effects of the sugar, the electronic structures of deglyco**1** and deglyco**2** were studied as a function of θ (see Figure 8 (black line, no symbol) for the relative energies and Figures S1 and S2 for the corresponding structures). As found for **1** and **2**, the global minimum for deglyco**1** and deglyco**2** contains an O−H···N7 hydrogen bond (≈1.75 Å). However, although the conformation of **1** and **2** with a planar nucleobase is a transition state, the global minimum for deglyco**1** and declyco**2** is planar (θ = 180°). This supports our proposal that the sugar influences the geometry of the nucleobase and is in agreement with previous findings for other modified nucleobases.[23] Two local minima are approximately 40 kJ mol^{-1} higher in energy, where the phenol group is twisted almost 25° from planarity with respect to the nucleobase to avoid repulsion with the N9 hydrogen. This is less than the 50° twist observed in the presence of the sugar moiety for the higher energy syn minima ($\theta \approx$ 55 and 305°), which suggests that the sugar not only introduces twist to the global minimum, but also increases the magnitude of the twist in the local minima.

The transition states connecting the local minima to the global minimum occur when the nucleobase and phenol ring are approximately perpendicular, where the corresponding θ rota-

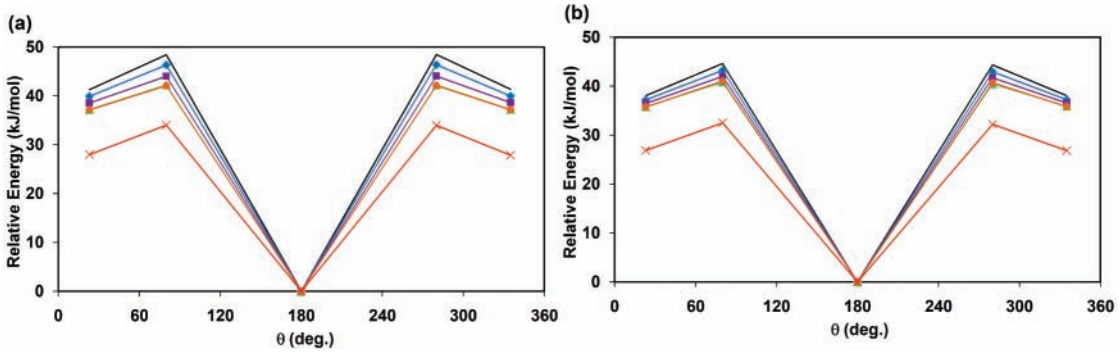

Figure 8. B3LYP/6-311+G(2df,p) relative energies of minima and transition states in gas phase (black, no symbol), cyclohexane (blue, ◆), chloroform (purple, ■), acetonitrile (green, ▲), DMSO (orange, ●), and water (red, ×) for (a) deglyco**1** and (b) deglyco**2** (see Figures S1 and S2 for geometrical information).

tional barriers are approximately 45−50 kJ mol^{-1}. It should be noted that the barrier to rotation is greater for the nucleobase than the deoxynucleoside, which implies that the sugar increases the conformational flexibility of the nucleobase. A transition state connecting the two twisted local minima could not be isolated, which we anticipate is due to steric crowding between the hydroxyl and the N9 hydrogen.

PCM single-point calculations were performed on the deglyco**1** and deglyco**2** structures in a variety of solvents (Figure 8). As described for adducts **1** and **2**, the twisted conformations are relatively more stable in more polar solvents, such as water. However, the planar structure is the global minimum in all solvents for deglyco**1** and deglyco**2**, including solvents with high polarity and/or hydrogen-bonding ability.

UV−vis spectra for deglyco**1** and deglyco**2** in water show absorption at ∼320 nm (Table 1), which is indicative of a planar conformation about θ. Previous studies on deglyco**1** in DMSO also reveal absorption at only ∼320 nm.[19] This contrasts the absorption at ∼280 nm for adducts **1** and **2**, which is indicative of a twisted structure. In addition, the phenolic OH protons of **1**[19] and **2** resonate at ∼δ 10.2 ppm in DMSO-d_6 (Figure S3, Supporting Information), while the corresponding protons of deglyco**1**[19] and deglyco**2** (Figure S4, Supporting Information) resonate at ∼δ 12.7 ppm. This downfield shift in the phenolic OH proton resonance, coupled with a 40 nm red-shift in the absorbance spectra (Table 1), is consistent with a planar hydrogen-bonded enol conformation for deglyco**1** and deglyco**2** in DMSO and a twisted (non-hydrogen bonded) conformation for **1** and **2**. Hence, both deglyco**1** and deglyco**2** undergo ESIPT in DMSO to form the keto structure with a fluorescence band at 460 nm, while **1** and **2** do not undergo ESIPT in DMSO and therefore give only enol emission at ∼395 nm. These experimental observations support our proposal that the steric effects of the sugar are responsible for the twist of the nucleobase.

Interestingly, despite the evidence (∼320 nm absorption) for the planar conformation of deglyco**1** discussed previously, only the enol tautomer emission ($\lambda \approx 390$ nm), but not the red-shifted emission (due to the keto tautomer), is observed for deglyco**1** in water.[19] For deglyco**2**, the red-shifted emission of ∼446 nm in water is due to the phenolate, which is weakly emissive (Table 1). Since the presence of the keto tautomer is dependent on the ability of the molecule to undergo ESIPT, which is dependent on the presence of the intramolecular hydrogen bond, we conclude that no O−H···N7 hydrogen bond is present in deglyco**1** in water despite its planar structure. Therefore, the water solvent must inhibit the tautomerization process by interrupting the intramolecular hydrogen bond. This experimental observation leads to the more general conclusion that protic solvents with hydrogen-bonding ability disrupt the O−H···N7 hydrogen bond in **1**. Although this proposal cannot be confirmed through our calculations since discrete hydrogen-bonding interactions were not included in our solvent model, it is interesting that the planar conformation of the nucleobase is favored in water despite evidence that there is no intramolecular hydrogen bonding to impede the flexibility of the nucleobase.

para-C8-Bonded Adducts. *(i) Nucleoside.* As discussed in the Introduction, we also considered the para-C8-bonded phenoxyl adducts of deoxyguanosine and deoxyadenosine (**3** and **4**), where our interest in these adducts stems from their potential use as pH sensors to study the electronic properties of the purines and as probes for carcinogenic phenoxyl radical damage to DNA.[24] Investigation of the para adducts also will yield additional structural information about the ortho adducts. Specifically, the significance of the O−H···N7 hydrogen bond, which is only present in the ortho adducts, for determining the preferred structure will be revealed. The present section will focus on the structure of the para adducts, and the structures of the ortho and para adducts will be compared in the concluding discussion.

Figures 2c,d display the B3LYP/6-31G(d) contour plots for rotation about θ and χ in **3** and **4**, respectively, which are similar for both purine adducts. Since many of the distortions found in the ortho adducts do not occur for the para adducts, the surfaces are greatly simplified, where no high-energy structures were left uncharacterized. Similar to the potential energy surfaces for the ortho adducts (Figures 2a,b), the surfaces for the para adducts have four syn minima, which include the global minimum, and two anti minima, which are approximately 30−40 kJ mol^{-1} higher in energy. In contrast to the ortho surface, the para surface is highly symmetric since rotation about θ by 180° simply changes the orientation of the hydroxyl group on the phenoxyl ring, which does not directly interact with the nucleobase or deoxyribose moiety.

The fully optimized minima and transition states on the potential energy surfaces for **3** and **4** are displayed in Figures 9 and 10, respectively, where χ, θ, and the sugar puckering generally do not deviate significantly from points identified in the contour plots. Closer examination of the structures reveals that all syn minima have O5′−H···N3 hydrogen bonds and that the structures are twisted about θ by approximately 40°. The two lower energy para syn minima are rotated about θ such that there is an interaction between a phenoxyl hydrogen and O4′. The two planar orientations of the phenoxyl and nucleobase rings are transition structures due to repulsion between hydrogens on the phenoxyl ring and C1′−H, and there are two higher energy transition states that involve a perpendicular arrangement of the nucleobase and phenoxyl rings. The similarities in the structures of the para syn minima and the lack of strong

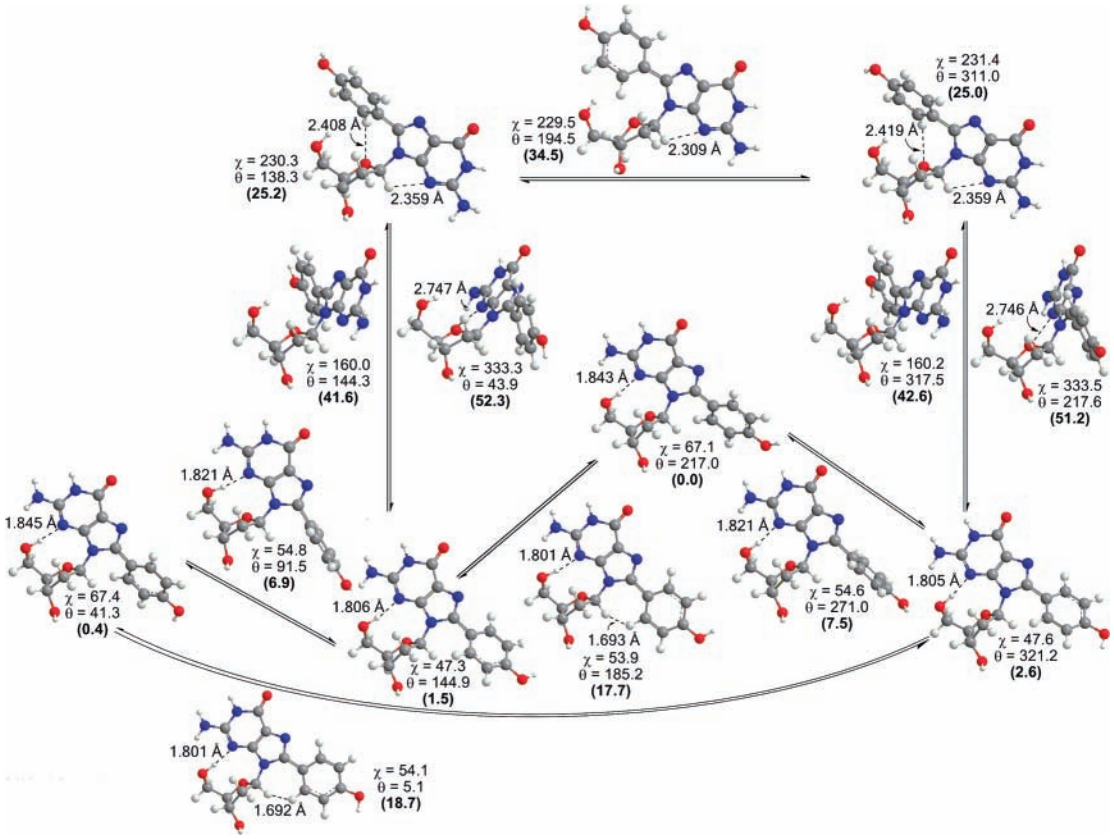

Figure 9. Selected bond lengths (Å) and dihedral angles (χ and θ, deg) for the minima and transition states of the C-bonded para-deoxyguanosine phenoxyl adduct (**3**) fully optimized with B3LYP/6-31G(d) (relative energies from B3LYP/6-311+G(2df,p) single-point calculations provided in parentheses, kJ mol^{-1}).

intramolecular interactions between the phenoxyl ring and the base or sugar moiety leads to very small (less than 3 kJ mol^{-1}) energy differences between minima and low rotational barriers (≈10−20 kJ mol^{-1}).

The two anti minima ($\chi \approx 230°$) contain interactions between O5′−H and the π-face of the phenoxyl ring and a C1′−H···N3 hydrogen bond. The sugar puckering in the anti minima is mainly the C1′−*exo*−C2′−*endo* twist, which improves the interaction between the C5′ group and the phenoxyl ring. The anti minima fall approximately 25 kJ mol^{-1} higher in energy than the global minimum, where the barrier for rotation between the anti minima is ≈10 kJ mol^{-1}. Four transition states connecting the syn and anti minima were identified, where there is a pair of transition states with χ values of ≈160 or 330° that differ in the orientation of the phenol hydroxyl group. The transition states at $\chi \approx 330°$ are 10 kJ mol^{-1} higher in energy due to repulsion between N3 and O4′.

Thus, our calculations predict that the preferred geometries of both **3** and **4** involve a twist about θ. This is supported by UV−vis and emission spectra in several solvents (Figure 11), which show absorption at ∼280 nm due to a twisted structure and no absorption at ∼320 nm that would correspond to a planar conformation. Furthermore, both **3** and **4** also show only enol emission at ∼390 nm (Figure 11 and Table 1). Because of our proposal that the sugar moiety imposes a twisted structure in the ortho adduct, we now consider the structure of the para adducts in the absence of the sugar moiety to determine whether the sugar indeed influences the structure.

(ii) Nucleobase. The potential energy surfaces for the deglycosylated versions of **3** and **4** (deglyco**3** and deglyco**4**) have two planar minima, which simply differ in the orientation of the phenol hydroxyl group (see Figures S7 and S8, Supporting Information, for relative energies and structures). The global minimum has the phenoxyl OH directed away from the N9 hydrogen and is only approximately 1 kJ mol^{-1} more stable than the local minimum. The minima are connected through two transition states that contain perpendicular arrangements of the phenoxyl and nucleobase rings. The planar minima identified for the para nucleobase adducts support our conclusion that the ortho adducts in water can adopt a planar conformation in the absence of the (solvated) O−H···N7 hydrogen bond.

The optical data shown in Table 1 support our computational findings. Specifically, the UV−vis spectra of deglyco**3** and deglyco**4** show planar absorption at ∼310 nm similar to the corresponding deglyco**1** and deglyco**2** ortho adducts. Furthermore, deglyco**3** and deglyco**4** also have only enol emission at ∼370−390 nm. It is important to note that, in contrast to **2** and deglyco**2**, no phenolate emission at ∼447 nm was observed for the corresponding para isomers **4** and deglyco**4**. Addition of base to **4** and deglyco**4** quenched fluoresecence, and a separate emission for the phenolate anion was not observed.[24] The fact that **4** and deglyco**4** are emissive in water at pH 7 (Table 1) also suggests that, unlike **2** and deglyco**2**, they do not undergo an ESP transfer process to form the phenolate anion, which would cause an appreciable drop in quantum yield. The proximity of the purine base to the phenolic OH in the ortho-dA isomers must play an important role in facilitating the ESP transfer process in water to generate the phenolate.

Overall, the computational and experimental studies on the C8-para adducts once again demonstrate the effect of the sugar on the preferred θ orientation, where deglyco**3** and deglyco**4** are planar, while **3** and **4** are twisted. The following section

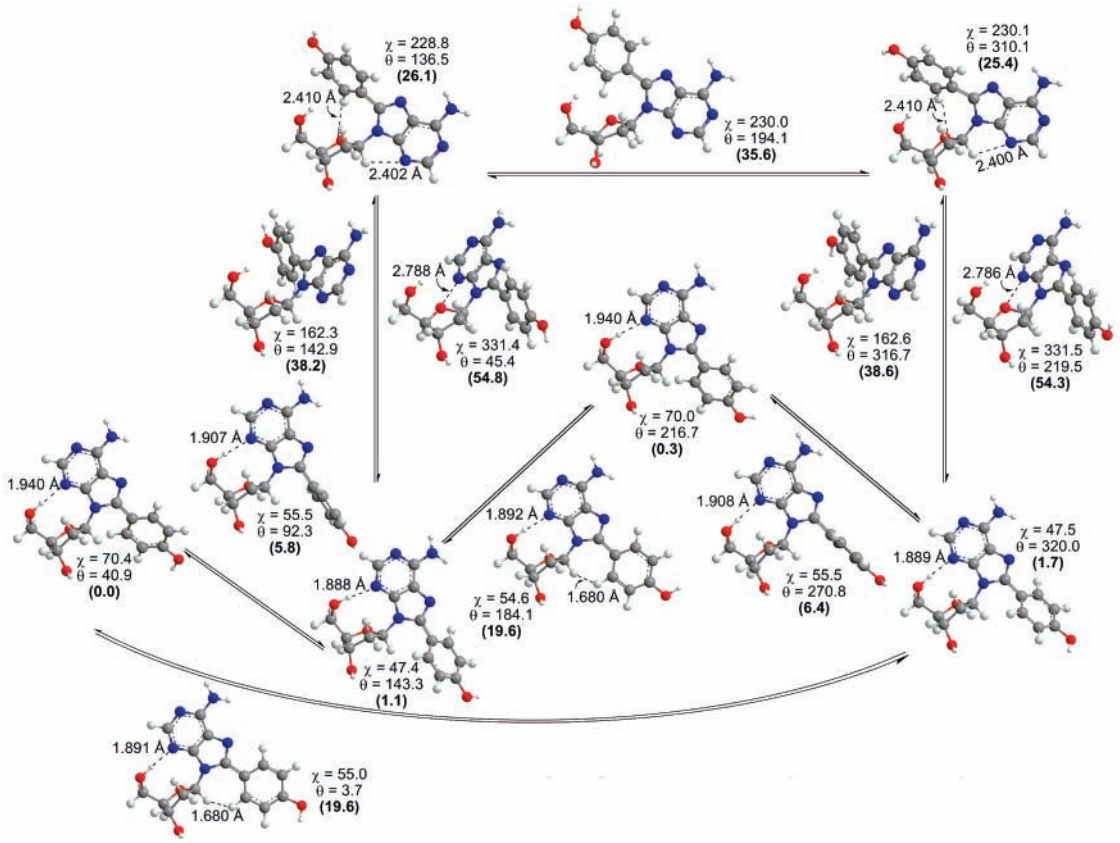

Figure 10. Selected bond lengths (Å) and dihedral angles (χ and θ, deg) for the minima and transition states of the C-bonded para-deoxyadenosine phenoxyl adduct (**4**) fully optimized with B3LYP/6-31G(d) (relative energies from B3LYP/6-311+G(2df,p) single-point calculations provided in parentheses, kJ mol^{-1}).

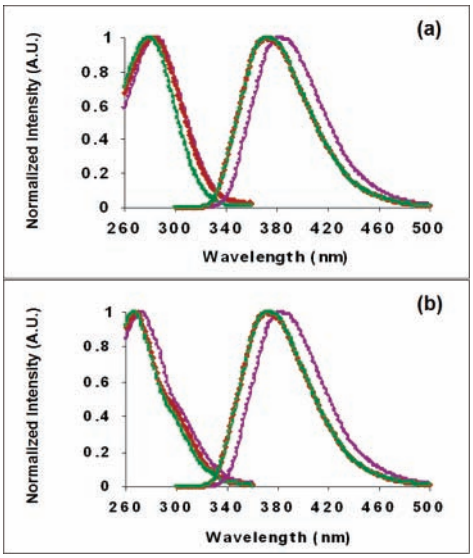

Figure 11. Normalized absorbance and emission spectra of adducts (a) **3** and (b) **4** in $CHCl_3$ (◆, brown), MeCN (■, green), and DMSO (●, purple).

will discuss further the implications of the structure of the para adducts for understanding the twist dependence in the ortho adducts.

Discussion

Comparison of the potential energy surfaces for the ortho- and para-deoxynucleoside adducts reveals important information about their structures. Specifically, both experiments and calculations indicate that the lowest energy conformers are twisted about the carbon−carbon bond connecting the phenoxyl ring to the nucleobase. Calculations reveal that the para syn minima are twisted about θ by approximately 40°, which is a considerably greater twist than the syn global minimum of the ortho adducts (25°) (Figure 12), but similar to the twist in the two higher energy ortho minima (∼50°). For comparison, the global minima on both the ortho and the para surfaces in the absence of the sugar moiety are planar, which suggests that the sugar moiety is inducing the twist within the nucleobase. The difference in the degree of twist in the ortho and para adducts in the presence of the sugar is explained by the competing factor of the O−H···N7 hydrogen bond, where only the lowest energy ortho adducts have this intramolecular interaction working to bring the nucleobase into a more planar conformation.

Interestingly, the para global minimum is approximately 20 kJ mol^{-1} higher in energy than the ortho global minimum, which is predominantly due to the loss of the O−H···N7 intramolecular hydrogen bond (Figure 12). This difference explains the shallower potential energy surface for the para adducts (Figures 2c,d) as compared to the ortho adducts (Figures 2a,b). Specifically, the ortho adducts with $\theta \approx 100-260°$ are greatly stabilized relative to the other conformers by the presence of an O−H···N7 hydrogen bond, which is absent in the remaining ortho structures ($\theta \approx 0-100$ and $260-360°$) and all para structures. As a result, the para adducts are much more flexible about θ, where even the transition states for rotation in the para nucleobases in the absence of the sugar are approximately 20 kJ mol^{-1} lower than those for the ortho adducts.

The previous discussion highlights the strong effect of the O−H···N7 hydrogen bond on the ground-state surface of the ortho adducts. Indeed, experimental results reveal that in some

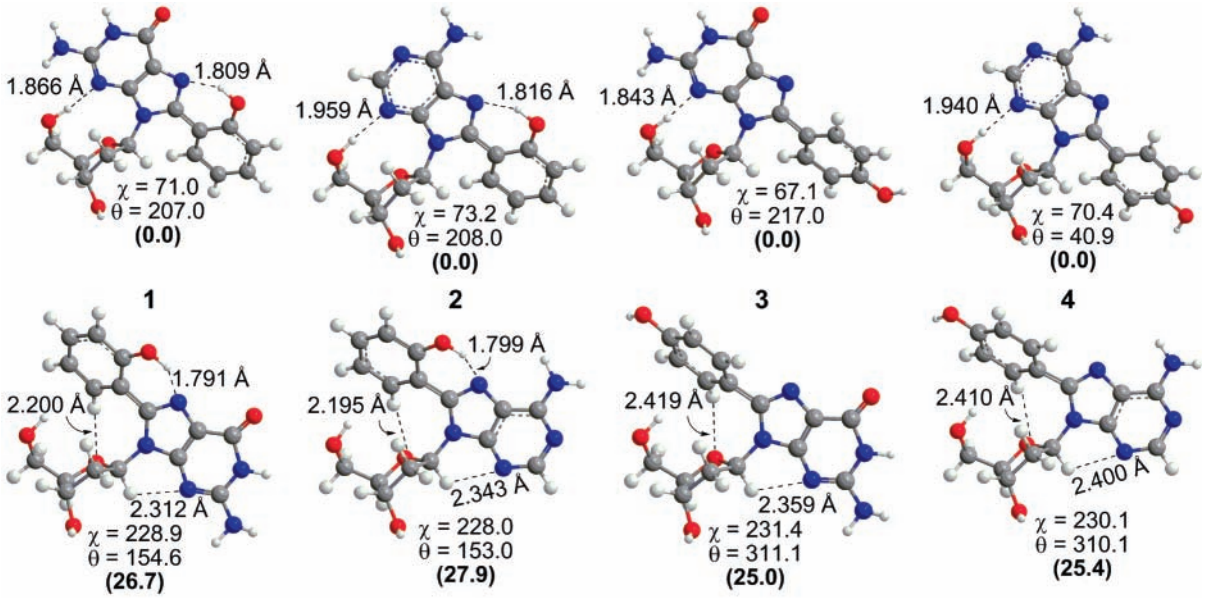

Figure 12. Selected bond lengths (Å) and dihedral angles (χ and θ, deg) for the global syn minima (top row) and lowest energy local anti minima (bottom row) fully optimized with B3LYP/6-31G(d) (relative energies from B3LYP/6-311+G(2df,p) single-point calculations provided in parentheses, kJ mol^{-1}).

TABLE 2: T/P Ratio for 1 and 2 in Various Aprotic Solvents[a]

solvent	T_{280}/P_{320} for **1** (% P)	T_{280}/P_{320} for **2** (% P)	solvent dipole moment (D)
$CHCl_3$	1.00 (50)	1.46 (41)	1.15
CH_2Cl_2	0.94 (52)	1.31 (43)	1.14
CH_3CN	1.20 (45)	1.72 (37)	3.44
hexane	2.43 (29)	2.56 (28)	0.08

[a] See text for an explanation of assumptions made to calculate the T/P ratios and Table S2 (Supporting Information) for molar absorption coefficients used in the calculations.

solvents, the hydrogen bond is strong enough to induce a planar conformation of the damaged deoxynucleoside. Therefore, in these solvents, the ground states of **1** and **2** are due to the presence of both twisted (T) and planar (P) conformers. Using the obtained molar absorption coefficients (ϵ) for **1**, **2**, deglyco**1**, and deglyco**2** (Table S2, Supporting Information), an estimate of the twisted/planar (T/P) ratio in the ground state can be made if it is assumed that (i) the ϵ values for **1** and **2** remain roughly constant between solvents, implying that an ϵ value for T can be approximated and (ii) ϵ values for P can be approximated from the results obtained for deglyco**1** and deglyco**2** where a planar conformation persists. With these hypotheses, the ϵ values for T ($\sim$17 800 cm^{-1} M^{-1} for **1** and $\sim$17 000 cm^{-1} M^{-1} for **2**) and P ($\sim$21 000 cm^{-1} M^{-1}) were used to approximate the T/P ratio in the ground state of **1** and **2** for different solvents (Table 2).

The calculated T/P ratios indicate that in aprotic solvents with a relatively large dipole moment, **1** exists in a $\sim$50:50 ratio between twisted and planar conformers. Furthermore, the results for different aprotic solvents are consistent with the previous discussion of the solvent effects, where the percent of structures with a planar conformation (% P) decreases as the dipole moment of the solvent increases. The T/P ratio is, however, much larger in the nonpolar aprotic solvent hexane, where the twisted orientation is further favored for both **1** and **2**. It appears that aprotic solvents with larger dipole moments ($CHCl_3$, CH_2Cl_2, and CH_3CN) interact with the dipole moment of the planar species to lower the ground-state energy, where the small dipole moment of hexane is less able to stabilize the more polar planar conformer. Calculations support this hypothesis, where the (gas phase) dipole moment of **1** is 6.939 when planar and 6.620 in the twisted global minimum.

The experiments suggest that the T/P ratios for **2** (Table 2) are larger than for **1**, which may be an artifact of the ϵ approximations made or suggest that a larger net dipole moment is created for **1** in comparison to **2** for the planar species. Indeed, the calculated dipole moments of **2** (1.953 when planar and 1.572 when twisted (global minimum)) are smaller, which makes sense due to the carbonyl functionality at O6 in **1**, which perturbs the electronic configuration in the planar conformer much more than the amino group at the corresponding position in **2**. These differences in the % P also could be attributed to the weaker O−H···N7 hydrogen-bond strength of **2**, which leads to a different solvent dependence (Figure 5).

Finally, it is noteworthy that the syn structure is the global minimum on the surfaces of **1**−**4** due to the presence of a strong O5′−H···N3 hydrogen bond. This may have implications for how the adducts interact with the complementary strands within DNA helices. Specifically, the anti orientation required for Watson−Crick hydrogen bonding may be possible in the DNA strand, or the syn orientation seen to be preferred in the nucleoside may readily occur, which could lead to mispairing. The implications of the preferred syn structure must be further considered in future work since the C5′ hydroxyl group in the nucleoside is replaced by a phosphodiester backbone in DNA, and therefore, the stabilizing (O5′−H···N3) hydrogen bond is not possible.

Conclusion

Our computational and experimental results demonstrate that the properties and structures of the ortho- and para-C-bonded phenoxyl adducts are not significantly dependent on the nature of the nucleobase. For both ortho and para damage, we found that the global minimum has a syn orientation about the glycosidic bond due to the presence of an O5′−H···N3 hydrogen bond and that the anti minimum is approximately 20−30 kJ mol^{-1} higher in energy. However, although both types of damaged nucleosides have a preferred twisted structure about

the carbon−carbon bond connecting the phenol and the nucleobase rings, the nucleobase adducts are planar. This suggests that the presence of the sugar introduces the twist into the structure. Nevertheless, the degree of the twist is less significant in the ortho global minimum as compared to the para due to the formation of an O−H···N7 hydrogen bond, which helps anchor the planar orientation. Calculated barriers between different conformers of the nucleosides and nucleobases suggest that the sugar also increases the nucleobase flexibility by lowering rotational barriers.

The competing effects of the sugar, which twists the nucleobase, and the O−H···N7 hydrogen bond, which anchors the planar conformation, lead to a strong solvent dependence of the ground-state structure of the ortho adducts. In hydrogen-bonding solvents (water), the keto tautomer is not formed when the nucleobase is excited, and there is only evidence for the twisted conformer of the nucleoside. Therefore, we conclude that solvents with hydrogen-bonding abilities must disrupt the intramolecular hydrogen bond (Scheme 2). However, there is evidence that the planar structure is stabilized in some solvents. Indeed, the ratio of twisted to planar conformers changes according to the properties of the solvent, where the ratio can be as large as 50:50 in some aprotic solvents.

In summary, the combined experimental and computational approach has given us a greater understanding of the structure of the ortho- and para-dA and dG C-bonded phenoxyl adducts. However, the implications of these findings within the context of DNA have not yet been explored fully. For example, the possibility of anti to syn conversion could create a potential for mispairing in the DNA strand, but whether the syn orientation is preferred in a larger model of a damaged oligonucleotide strand remains to be investigated. Additionally, the possibility of enhanced abasic site formation post-damage is a cause for concern since the effects of the damage on the stability of the glycosidic bond are uncertain.

Acknowledgment. Support for this research was provided by the Natural Sciences and Engineering Research Council (NSERC) of Canada, the Canada Research Chair program, the Canada Foundation for Innovation, the University of Guelph, and the Ontario Innovation Trust Fund. A.L.M. thanks NSERC and the Alberta Ingenuity Fund for postgraduate scholarships. R.A.M. thanks Alireza Omumi and Katherine Schlitt for carrying out preliminary experiments.

Supporting Information Available: Figures S1−S8 and Tables S1 and S2 as described in the text. This material is available free of charge via the Internet at http://pubs.acs.org.

References and Notes

(1) Kool, E. T. *Acc. Chem. Res.* **2002**, *35*, 936−943.
(2) Lynch, S. R.; Liu, H. B.; Gao, J. M.; Kool, E. T. *J. Am. Chem. Soc.* **2006**, *128*, 14704−14711.
(3) Ogawa, A. K.; Abou-Zied, O. K.; Tsui, V.; Jimenez, R.; Case, D. A.; Romesberg, F. E. *J. Am. Chem. Soc.* **2000**, *122*, 9917−9920.
(4) Leumann, C. J. *Bioorg. Med. Chem.* **2002**, *10*, 841−854.
(5) Cadet, J.; Douki, T.; Gasparutto, D.; Ravanat, J. L. *Mutat. Res.* **2003**, *531*, 5−23.
(6) Frederico, L. A.; Kunkel, T. A.; Shaw, B. R. *Biochemistry* **1993**, *32*, 6523−6530.
(7) Robertson, K. D.; Jones, P. A. *Carcinogenesis* **2000**, *21*, 461−467.
(8) Josephy, P. D.; Mannervik, B. *Molecular Toxicology*, 2nd ed.; Oxford University Press, Inc.: New York, 2006; pp 46−82.
(9) Faucet, V.; Pfohl-Leszkowicz, A.; Dai, J.; Castegnaro, M.; Manderville, R. A. *Chem. Res. Toxicol.* **2004**, *17*, 1289−1296.
(10) Gannett, P. M.; Lawson, T.; Miller, M.; Thakkar, D. D.; Lord, J. W.; Yau, W. M.; Toth, B. *Chem.-Biol. Interact.* **1996**, *101*, 149−164.
(11) Rogan, E. G.; Cavalieri, E. L.; Tibbels, S. R.; Cremonesi, P.; Warner, C. D.; Nagel, D. L.; Tomer, K. B.; Cerny, R. L.; Gross, M. L. *J. Am. Chem. Soc.* **1988**, *110*, 4023−4029.
(12) Dai, Q.; Xu, D. W.; Lim, K.; Harvey, R. G. *J. Org. Chem.* **2007**, *72*, 4856−4863.
(13) Dai, J.; Sloat, A. L.; Wright, M. W.; Manderville, R. A. *Chem. Res. Toxicol.* **2005**, *18*, 771−779.
(14) Dai, J.; Wright, M. W.; Manderville, R. A. *Chem. Res. Toxicol.* **2003**, *16*, 817−821.
(15) Dai, J.; Wright, M. W.; Manderville, R. A. *J. Am. Chem. Soc.* **2003**, *125*, 3716−3717.
(16) Manderville, R. A. *Can. J. Chem.* **2005**, *83*, 1261−1267.
(17) Kikugawa, K.; Kato, T.; Kojima, K. *Mutat. Res.* **1992**, *268*, 65−75.
(18) Hiramoto, K.; Kojima, K.; Kato, T.; Kikugawa, K. *Mutat. Res.* **1992**, *272*, 259−260.
(19) McLaughlin, C. K.; Lantero, D. R.; Manderville, R. A. *J. Phys. Chem. A* **2006**, *110*, 6224−6230.
(20) Mosquera, M.; Penedo, J. C.; Rodriguez, M. C. R.; Rodriguez Prieto, F. *J. Phys. Chem.* **1996**, *100*, 5398−5407.
(21) Henary, M. M.; Fahrni, C. J. *J. Phys. Chem. A* **2002**, *106*, 5210−5220.
(22) Abou-Zied, O. K.; Jimenez, R.; Thompson, E. H. Z.; Millar, D. P.; Romesberg, F. E. *J. Phys. Chem. A* **2002**, *106*, 3665−3672.
(23) Bardon, A. B.; Wetmore, S. D. *J. Phys. Chem. A* **2005**, *109*, 262−272.
(24) Sun, K. M.; McLaughlin, C. K.; Lantero, D. R.; Manderville, R. A. *J. Am. Chem. Soc.* **2007**, *129*, 1894−1895.
(25) O'Neill, M. A.; Dohno, C.; Barton, J. K. *J. Am. Chem. Soc.* **2004**, *126*, 1316−1317.
(26) Guest, C. R.; Hochstrasser, R. A.; Sowers, L. C.; Millar, D. P. *Biochemistry* **1991**, *30*, 3271−3279.
(27) Allan, B. W.; Reich, N. O.; Beechem, J. M. *Biochemistry* **1999**, *38*, 5308−5314.
(28) *Spartan '02*; Wavefunction, Inc.: Irvine, CA, 2002.
(29) Systematic searches also were performed on the ortho-deoxyguanosine adduct (**1**), which resulted in the same global minimum as the Monte Carlo search. Consequently, only Monte Carlo searches were performed for the remaining adducts.
(30) Frisch, M. J.; Trucks, G. W.; Schlegel, H. B.; Scuseria, G. E.; Robb, M. A.; Cheeseman, J. R.; Montgomery, J. A., Jr.; Vreven, T.; Kudin, K. N.; Burant, J. C.; Millam, J. M.; Iyengar, S. S.; Tomasi, J.; Barone, V.; Mennucci, B.; Cossi, M.; Scalmani, G.; Rega, N.; Petersson, G. A.; Nakatsuji, H.; Hada, M.; Ehara, M.; Toyota, K.; Fukuda, R.; Hasegawa, J.; Ishida, M.; Nakajima, T.; Honda, Y.; Kitao, O.; Nakai, H.; Klene, M.; Li, X.; Knox, J. E.; Hratchian, H. P.; Cross, J. B.; Bakken, V.; Adamo, C.; Jaramillo, J.; Gomperts, R.; Stratmann, R. E.; Yazyev, O.; Austin, A. J.; Cammi, R.; Pomelli, C.; Ochterski, J. W.; Ayala, P. Y.; Morokuma, K.; Voth, G. A.; Salvador, P.; Dannenberg, J. J.; Zakrzewski, V. G.; Dapprich, S.; Daniels, A. D.; Strain, M. C.; Farkas, O.; Malick, D. K.; Rabuck, A. D.; Raghavachari, K.; Foresman, J. B.; Ortiz, J. V.; Cui, Q.; Baboul, A. G.; Clifford, S.; Cioslowski, J.; Stefanov, B. B.; Liu, G.; Liashenko, A.; Piskorz, P.; Komaromi, I.; Martin, R. L.; Fox, D. J.; Keith, T.; Al-Laham, M. A.; Peng, C. Y.; Nanayakkara, A.; Challacombe, M.; Gill, P. M. W.; Johnson, B.; Chen, W.; Wong, M. W.; Gonzalez, C.; Pople, J. A. *Gaussian 03*, Revisions C.02 and D.01; Gaussian, Inc.: Pittsburgh, PA, 2004.
(31) Sanders, J. K. M.; Hunter, B. K. *Modern NMR Spectroscopy*; Oxford University Press: Oxford, 1987; pp 93−207.
(32) Gillet, L. C. J.; Scharer, O. D. *Org. Lett.* **2002**, *4*, 4205−4208.
(33) Gannet, P. M.; Sura, T. P. *Synth. Commun.* **1993**, *23*, 1611−1615.
(34) Patterson, G. S. *J. Chem. Educ.* **1999**, *76*, 395−398.
(35) Western, E. C.; Daft, J. R.; Johnson, E. M.; Gannet, P. M.; Shaughnessy, K. H. *J. Org. Chem.* **2003**, *68*, 6767−6774.
(36) A small number of points throughout the main part of the surfaces also could not be optimized under geometrical constraints; however, since realistic structures for the six to eight points surrounding the missing structures could be obtained easily, the energies for the problematic structures were extrapolated to produce a smooth curve.
(37) Polak, M.; Seley, K. L.; Plavec, J. *J. Am. Chem. Soc.* **2004**, *126*, 8159−8166.
(38) Gannett, P. M.; Sura, T. P. *Chem. Res. Toxicol.* **1993**, *6*, 690−700.
(39) Eason, R. G.; Burkhardt, D. M.; Phillips, S. J.; Smith, D. P.; David, S. S. *Nucleic Acids Res.* **1996**, *24*, 890−897.
(40) Dutta, S.; Li, Y.; Johnson, D.; Dzantiev, L.; Richardson, C. C.; Romano, L. J.; Ellenberger, T. *Proc. Natl. Acad. Sci. U.S.A.* **2004**, *101*, 16186−16191.